Spectral and Crystallographic Coincidence in a Mixed Crystal of Two Components and a Crystal of Their Hybrid Component in Pyrrolopyrrole Pigments

J. Mizuguchi* and H. Shikamori

Department of Applied Physics, Graduate School of Engineering, Yokohama National University, 79-5 Tokiwadai, Hodogaya-ku, 240-8501 Yokohama, Japan

Received: June 18, 2003; In Final Form: October 21, 2003

Diketopyrrolopyrroles are typical hydrogen-bonded pigments of red color on the basis of the skeleton of 1,4-diketo-3,6-diphenylpyrrolo[3,4-*c*]pyrrole (DPP). Our previous investigation revealed that the 1:1 mixed crystal (MX-DPP) composed of DPP and its *tert*-butylphenyl derivative (BTB-DPP) gives practically the same electronic spectra as well as X-ray diffraction diagrams as those of the hybrid compound (MTB-DPP) of DPP and BTB-DPP. To elucidate the above coincidence, electronic structure has been studied in the present investigation in evaporated films and single crystals of MX-DPP and MTB-DPP with major focus on the crystal structure and intermolecular interactions. According to the structure analysis, the space groups of both crystals are the same ($P\bar{1}$) and the crystallographic parameters are also quite similar. In both crystals, the same molecular environment (in other words, "local similarity") prevails throughout the crystal as characterized by two pairs of "*tert*-butyl group and phenyl ring". These facts lead us to conclude that the local similarity is the determinant for the coincidence of the crystallographic and electronic structures.

1. Introduction

Diketopyrrolopyrrole pigments are industrially important red pigments on the basis of the skeleton of 1,4-diketo-3,6-diphenylpyrrolo[3,4-*c*]pyrrole (abbreviated to DPP, Figure 1).[1,2] DPPs have also attracted attention as colorants for imaging areas as well as color filters of liquid crystal displays (LCD). These DPP pigments are typically characterized by intermolecular hydrogen bonds between the NH group of one molecule and the O atom of the neighboring one. This H-bond network causes the very good thermal and solvent resistance of the materials.

Figure 1 shows three kinds of DPP derivatives: DPP,[3] its bis(4-*tert*-butylphenyl) derivative (BTB-DPP),[4] and its mono-(4-*tert*-butylphenyl) derivative (MTB-DPP).[5] Both DPP and BTB-DPP are symmetrical molecules, whereas MTB-DPP is an asymmetrical one characterized by a hybrid structure of DPP and BTB-DPP. In our previous investigation, DPP and BTB-DPP form a 1:1 mixed crystal (MX-DPP) and its spectroscopic and crystallographic behavior is surprisingly similar to that of MTB-DPP.[6,7] The present phenomenon is scientifically of great interest why two symmetrical molecules give the same optical and structural properties in the solid state as those of the asymmetrical one. At the same time, this outstanding effect also makes sense from the practical point of view, because the mixed crystal based on two kinds of inexpensive symmetrical molecules gives the same color as that of expensive asymmetric molecules. For these reasons, an attempt was made in the present investigation to clarify the electronic structure of MX-DPP and MTB-DPP in both evaporated films and single crystals.

In regard to the mechanism of the above coincidence in optical and structural properties, Karfunkel, Mizuguchi, and others simulated the crystal structures of MX-DPP and MTB-DPP by optimizing the geometry and minimizing the packing energy and proposed a model called local similarity as shown in Figure 2.[8] This picture illustrates the simulated molecular arrangement of MX-DPP and MTB-DPP. In each lattice plane, the *tert*-butyl group of one molecule faces the phenyl ring of the neighboring one in both compounds. The area surrounded by dotted circles is called local similarity and is held throughout the crystal. Then, the molecular environment in both MX-DPP and MTB-DPP is practically the same and is expected to give nearly the same spectroscopic and crystallographic properties. Since these solid-state properties are so dependent on the molecular structure and arrangement, it is necessary to determine the crystal structure to fully elucidate the mechanism of the coincidence of these physical properties.

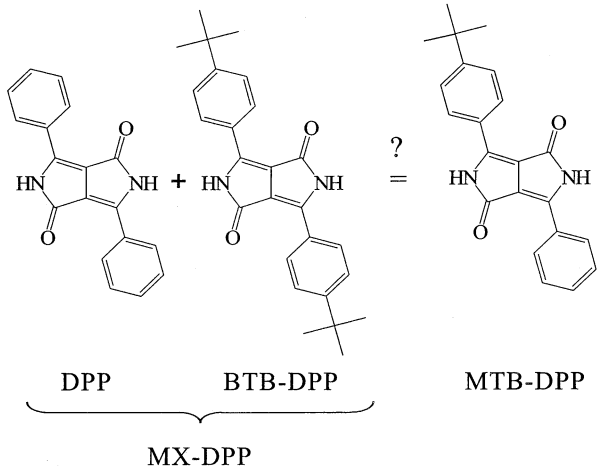

Figure 1. Schematic diagram for MX-DPP and MTB-DPP.

The present paper is composed of two parts. The first part describes the coincidence of electronic spectra and X-ray diffraction diagrams in evaporated films. The second part deals with the crystal structure and polarized reflection spectra measured on single crystals.

* Address correspondence to this author.

10.1021/jp030764b CCC: $27.50
Published on Web 01/22/2004

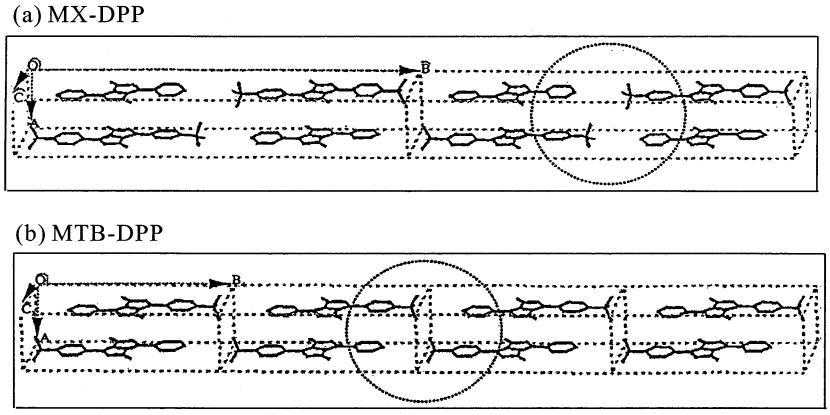

Figure 2. Molecular arrangement of simulated MX-DPP and MTB-DPP.[8] The crystal parameters are given in Table 1.

2. Experimental Section

2.1. Materials and Sample Preparations. DPP and BTB-DPP were obtained from Ciba Specialty Chemicals. MTB-DPP was synthesized according to the method described in ref 7.

DPP, BTB-DPP, and MTB-DPP were purified once by vacuum sublimation using a two-zone furnace.[9] MX-DPP was then prepared by dissolving both DPP and BTB-DPP in dimethylsulfoxide (DMSO) through deprotonation with sodium hydroxide, followed by protonation with hydrochloric acid for the precipitation.[7] After that, the MX-DPP was purified by sublimation using the above apparatus.

Evaporated thin films of MX-DPP and MTB-DPP were prepared onto glass substrates (film thickness: about 1000 Å) using conventional vacuum evaporation equipment (Tokyo Vacuum Co. Ltd.: model EG240). Plain glass slides were used as the substrate for measurements for visible absorption spectra, IR-spectra, and X-ray diffraction diagrams, respectively. Vapor treatment of MX-DPP and MTB-DPP was carried out by exposing the evaporated films to acetone vapor for about 15 h to induce molecular rearrangement.

A solid-state reaction in evaporated films was also carried out for the formation of the mixed crystal by means of an Ar^+-laser ("heat mode"). A multilayer of evaporated films composed of four pairs of alternating DPP (ca. 150 Å) and BTB-DPP (ca. 150 Å) was prepared on a glass substrate by successive evaporation of each material under high vacuum (total thickness: about 1200 Å). A protection layer of a photopolymer (SD17 from DIC) was applied by spin coating. This protection layer was extremely important to prevent the material from being evaporated during the solid-state reaction by laser. The reaction was initiated by an Ar^+ laser beam (514 nm: 400 mW/cm^2) with a scanning rate of 100, 125, 150, 175, 200, and 225 mm/sec. The resulting spectral changes were measured by means of a microscope spectrometer described below.

Single crystals of MX-DPP and MTB-DPP were grown from the vapor phase in a closed system, using a two-zone furnace. MX-DPP was sublimed at about 740 K. After 60 h of vapor growth, several plateletlike crystals were obtained. In a similar way, the single crystals of MTB-DPP were obtained at a sublimation temperature of around 620 K.

2.2. Equipment and Measurements. UV−vis spectra and photoluminescence spectra were recorded on a UV-2400PC spectrophotometer (Shimadzu) and a F4500 fluorescent spectrometer (Hitachi), respectively. The temperature dependence of the absorption spectra in evaporated films were measured in the range between 12 and 293 K on a UV-2400PC spectrophotometer in combination with a cryostat from Iwatani Gas Co. Ltd. (model: CRT-105-OP). The photoluminescence spectra were measured under the excitation of monochoromatic light of 365 nm. Measurements for polarized reflection spectra were made on single crystals by means of a UMSP80 microscope spectrophotometer (Carl Zeiss). An Epiplan Pol (×8) objective was used together with a Nicol-type polarizer. Reflectivities were corrected relative to the reflection standard of silicon carbide.

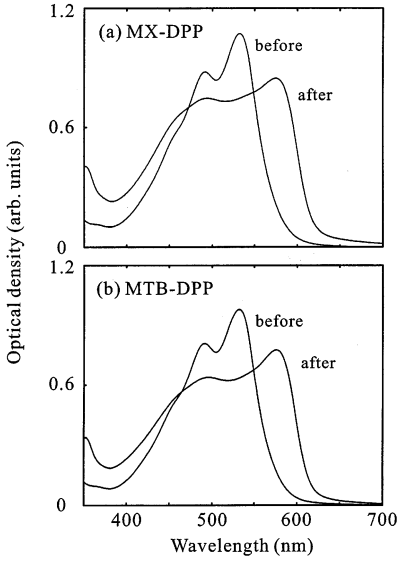

Figure 3. Solid-state spectra in evaporated films for MX-DPP and MTB-DPP before and after vapor treatment.

2.3. Molecular Orbital (MO) Calculations. The INDO/S program used for spectroscopic calculations is part of the ZINDO program package.[10] Optical absorption bands for the molecule in crystal were calculated on the basis of the X-ray *x*, *y*, and *z* coordinate sets using the INDO/S Hamiltonian.

3. Results and Discussion

3.1. Similarities in Electronic Spectra and X-ray Diffraction Diagrams in Evaporated Films. *Solid-State Spectra in Evaporated Films.* Figure 3 shows the solid-state spectra of evaporated films for MX-DPP and MTB-DPP before and after vapor treatment, respectively. The absorption spectra in both samples before and after vapor treatment are remarkably similar to each other. The absorption spectra before vapor treatment are typical of DPP derivatives peaking at about 540 nm.[2] However, the longer-wavelength band is then displaced toward longer wavelengths around 580 nm when the evaporated films are exposed to acetone vapor for about 15 h. As a consequence, the color changes from vivid red to bluish red and the resulting

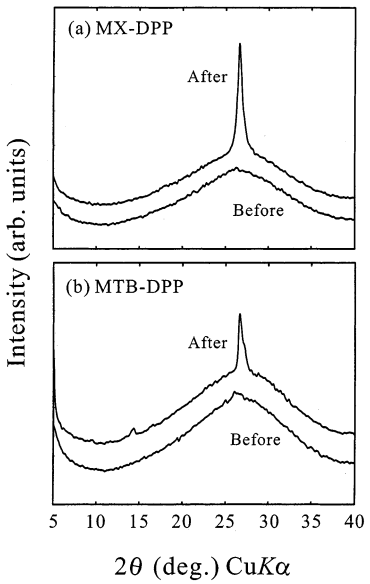

Figure 4. X-ray diffraction diagrams in evaporated films for MX-DPP and MTB-DPP before and after vapor treatment.

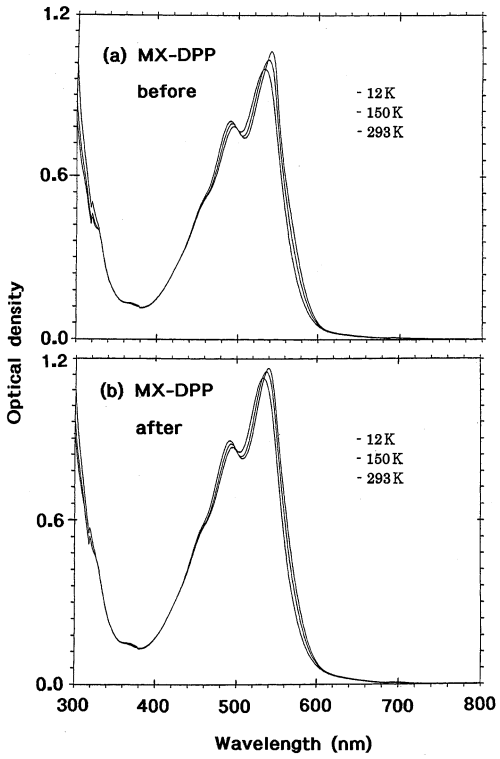

Figure 5. Temperature dependence of absorption spectra of evaporated MX-DPP and MTB-DPP before vapor treatment.

spectral shape is quite unusual as compared with that of ordinary pyrrolopyrroles.

X-ray Diffraction Diagrams. Figure 5 shows the X-ray diffraction diagrams of evaporated MX-DPP and MTB-DPP before and after vapor treatment. The broad diffraction band around 26° is due to the glass substrate used. No noticeable diffraction peaks are recognized in both samples before vapor treatment, suggesting that the phase is rather amorphous. However, in this state, the intermolecular hydrogen bonds between the NH group of one molecule and the O atom of the neighboring one are formed on the molecular plane in both samples, as revealed from IR spectra presented later. Then, vapor treatment brings about crystallization in both samples as shown

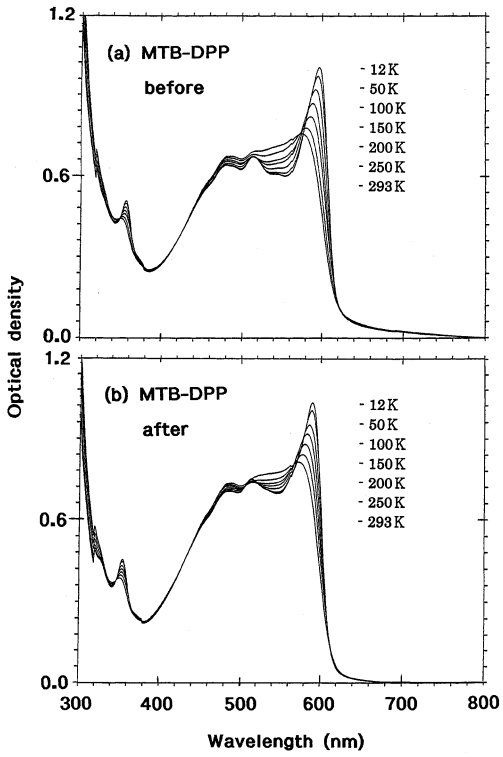

Figure 6. Temperature dependence of absorption spectra of evaporated MX-DPP and MTB-DPP after vapor treatment.

by the appearance of the diffraction peak around 26° (interplanar distance: about 3.5 Å). This indicates that the molecules are ordered along the stacking axis because of vapor treatment, causing the spectral change to occur. In this way, the molecules are fully stabilized not only on the molecular plane because of NH···O hydrogen bonds, but also along the stacking axis because of $\pi-\pi$ interactions.

Figure 5a and b shows the temperature dependence of absorption spectra of evaporated MX-DPP before and after vapor treatment, respectively. Likewise, the temperature dependence of evaporated MTB-DPP is shown in Figure 6 a and b. The temperature dependence of both samples before and after vapor treatment behaves exactly in the same way. The absorption spectra before vapor treatment exhibit insignificant temperature dependence while the longest-wavelength band after vapor treatment in both compounds are remarkably temperature-dependent. The present result is closely related to the nature of the absorption band as discussed later.

IR Spectra in Evaporated Films. The IR spectra in evaporated films of MX-DPP and MTB-DPP before and after vapor treatment are shown in Figure 7, respectively. In both compounds, no significant effect due to vapor treatment is recognized and the IR spectra are quite similar to each other. The vibrational band around 3100 cm^{-1} is assigned to the NH stretching. This band is quite broad as compared with the free NH stretching band (about 3500 cm^{-1}) and is considerably displaced toward lower wavenumbers together with the C═O stretching band around 1640 cm^{-1}. This is due to the formation of NH···O intermolecular hydrogen bonds (between the NH group of one molecule and the O atom of the neighboring one) that stabilizes the C═O and NH stretchings. It is also remarkable to note that there are two absorption bands for the C═O stretching, as typically characterized by asymmetric MTB-DPP with two carbonyl groups and also by a pair of symmetric DPP and BTB-DPP (MX-DPP) which possess their own carbonyl group.

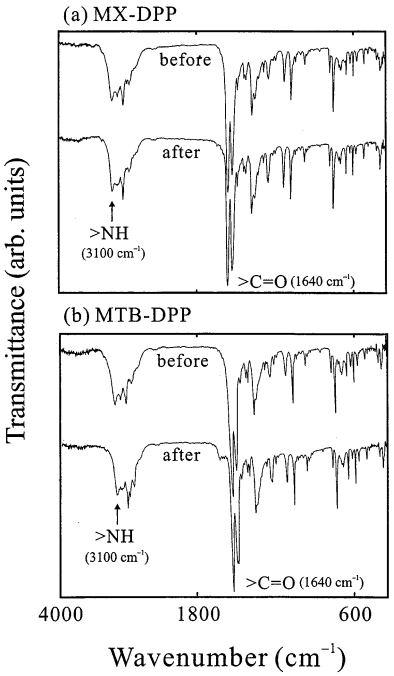

Figure 7. IR-spectra in evaporated films before and after vapor treatment: (a) MX-DPP and (b) MTB-DPP.

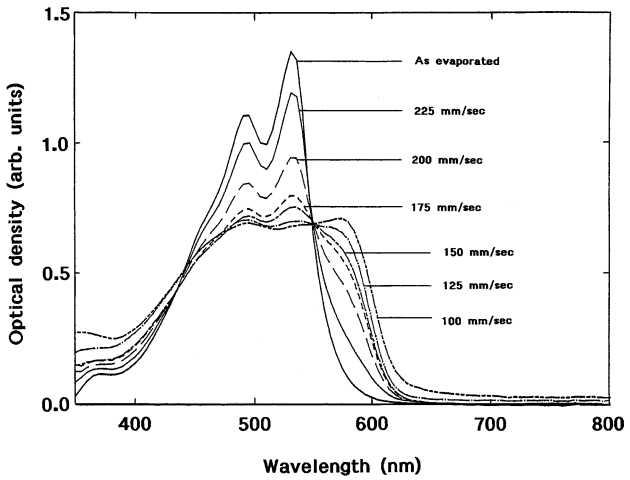

Figure 8. Spectral changes of the evaporated multilayers composed of alternating DPP (4 × 150 Å) and MTB-DPP (4 × 150 Å) as a function of the scanning rate of an Ar^+ laser: 100, 125, 150, 175, 200, and 225 mm/s. Ar^+ laser: 514 nm with a power of 400 mW/cm^2.

MX-DPP Formed by a Solid-State Reaction in Evaporated Films. Figure 8 shows the spectral changes of the evaporated multilayers composed of alternating DPP (4 × 150 Å) and MTB-DPP (4 × 150 Å) as a function of the scanning rate of an Ar^+ laser. The absorption spectrum before irradiation coincides with the vapor-untreated spectrum of MX-DPP shown in Figure 3a. Then, an absorption shoulder (i.e., incipient formation of an absorption band) begins to appear around 580 nm under irradiation of an Ar^+ laser with a scanning rate of 225 mm/s while the intensity of the two absorption bands around 480 and 540 nm is decreased. The new band grows to an absorption band around 580 nm with increasing power (i.e., slower scanning rate), accompanied by an isosbestic point around 550 nm. The final absorption band agrees with the band of MX-DPP after vapor treatment shown in Figure 3a. The present spectral transition clearly indicates the final absorption spectrum comprises three absorption bands: original two bands around 480 and 540 and one additional band around 580 nm. Then, it is more reasonable to assign the longest-wavelength band (ca. 580 nm) in Figure 3a as a new band rather than a bathochromically displaced band of 540 nm because of vapor treatment.

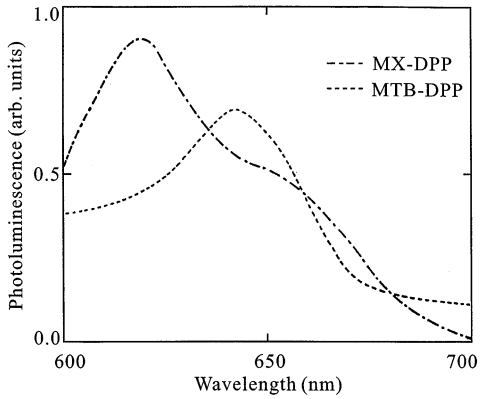

Figure 9. Photoluminescence spectra of powdered MX-DPP and MTB-DPP.

Photoluminescence Spectra Measured on Powders. In contrast to the coincidence in electronic spectra and X-ray diffraction diagrams presented so far, a clear difference is now recognized in photoluminescence between MX-DPP and MTB-DPP. Figure 9 shows the photoluminescence spectra of powdered MX-DPP and MTB-DPP. In MX-DPP, the photoluminescence is observed around 620 nm, accompanied by a shoulder around 660 nm, whereas the emission maximum occurs around 645 nm in MTB-DPP. The emission spectrum of MX-DPP is a mirror image of the absorption spectrum shown in Figure 3 (after vapor treatment) and is characterized by a relatively small Stokes shift. On the other hand, a large Stokes shift is observed in MTB-DPP as shown by the emission maximum around 645 nm. This indicates that the potential minimum of the excited state is significantly displaced relative to the potential minimum of the ground state in MTB-DPP. The mechanism of this phenomenon is, however, not yet clarified.

3.2. Structural and Spectroscopic Properties in Single Crystals. *Crystal Structures of MX-DPP and MTB-DPP*. Table 1 details the crystallographic parameters for MX-DPP[5] and MTB-DPP[11] together with those of the simulated ones,[8] whereas those of DPP and BTB-DPP (component molecules for MX-DPP) are shown in Table 2 as the reference. The space groups of both MX-DPP and BTB-DPP are the same ($P\bar{1}$) and the crystallographic parameters are quite similar as shown in Table 1. It is apparent that the structure of MX-DPP is isomorphous with that of MTB-DPP. In addition, the space group experimentally obtained for MX-DPP and MTB-DPP agrees with that of simulated ones ($P\bar{1}$). The lattice parameters are also quite similar to each other, although the *c* lattice of the simulated MX-DPP is nearly twice as long as that of the experimental one. MX-DPP and MTB-DPP crystallize in completely different lattices from those of DPP and BTB-DPP (Table 2). This indicates that DPP (or BTB-DPP) is not isomorphously substituted into the BTB-lattice (or DPP).

An ORTEP plot is shown in the Figure 10 for MX-DPP. Both DPP and BTB-DPP molecules have a molecular symmetry of C_i. The two phenyl rings on each side of the heterocyclic ring system are twisted symmetrically in the same direction: 13° in DPP and 10° in BTB-DPP with respect to the heterocyclic system. Figure 11 a shows the molecular arrangement in MX-DPP along the stacking axis. The molecular stack is composed of two kinds of two-dimensional H-bond layers: one is based on DPP molecules and the other is based on BTB-DPP molecules as shown in Figure 11b. On each molecular plane,

TABLE 1: Crystallographic Parameters for MX-DPP and MTB-DPP

	MX-DPP		MTB-DPP	
	experimental	simulated[a]	experimental	simulated[a]
molecular formula	$C_{18}H_{12}N_2O_2 + C_{26}H_{28}N_2O_2$	$C_{18}H_{12}N_2O_2 + C_{26}H_{28}N_2O_2$	$C_{22}H_{20}N_2O_2$	$C_{22}H_{20}N_2O_2$
crystal system	triclinic	triclinic	triclinic	triclinic
space group	$P\bar{1}$	$P\bar{1}$	$P\bar{1}$	$P\bar{1}$
Z	2	4	2	2
molecular weight	688.81	688.81	344.41	344.41
molecular symmetry	C_i	C_i	C_1	C_1
a (Å)	6.57(1)	6.7	6.45(2)	6.7
b (Å)	7.25(2)	7.3	7.09(4)	7.3
c (Å)	18.36(4)	37.0	17.95(6)	18.5
α (deg)	83.5(2)	95.8	84.9(4)	95.0
β (deg)	82.4(2)	90.0	86.1(1)	89.1
γ (deg)	87.0(2)	89.5	87.4(4)	89.1

[a] Reference 8. The unit cell has been transformed in accordance with the standard setting.

TABLE 2: Crystallographic Parameters for DPP and BTB DPP

	DPP[a]	BTB-DPP[b]
molecular formula	$C_{18}H_{12}N_2O_2$	$C_{26}H_{28}N_2O_2$
crystal system	triclinic	triclinic
space group	$P\bar{1}$	$P\bar{1}$
Z	1	2
molecular weight	288.310	400.52
molecular symmetry	C_i	C_1
a (Å)	3.817(1)	9.872(1)
b (Å)	6.516(1)	15.779(1)
c (Å)	13.531(2)	7.228(1)
α (deg)	93.11(1)	96.31(1)
β (deg)	86.97(1)	91.13(1)
γ (deg)	95.02(1)	82.20(1)

[a] Reference 3. [b] Reference 4.

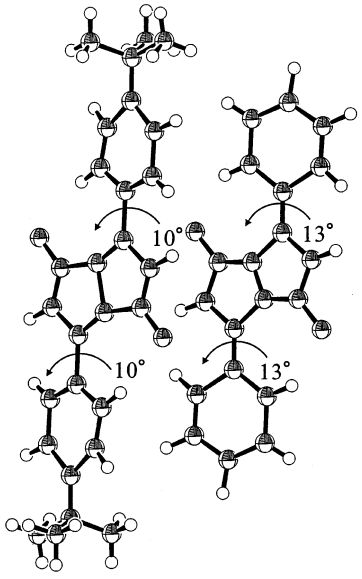

Figure 10. Molecular conformation of MX-DPP.

there are chains of intermolecular hydrogen bonds, along the *b*-axis, between the NH group of one DPP (or BTB-DPP) molecule and the O atom of the neighboring DPP (or BTB-DPP) molecule. The present H-bond network is typical of all DPP pigments[1−5] and causes the very good thermal and solvent resistance of the hydrogen-bonded DPP pigments. Both DPP and BTB-DPP molecules are alternately stacked in a fashion "bricks in a brick wall" which is reminiscent of the J-aggregate structure of cyanine dyestuffs[12] as well as the structure of biphenyl DPP[13] and thionated DPP.[14,15]

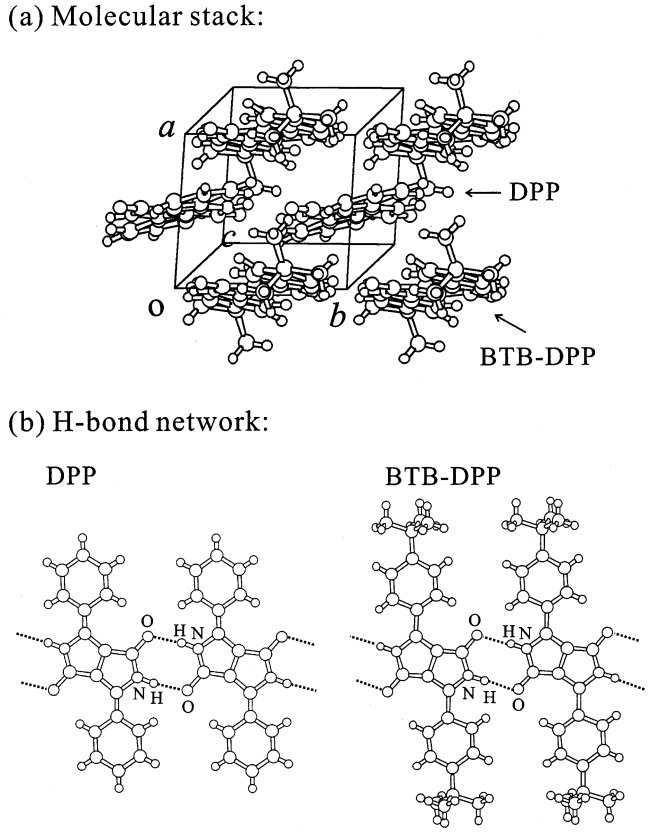

Figure 11. (a) Molecular stack in MX-DPP and (b) H-bond network of DPP and BTB-DPP on the molecular plane.

An ORTEP plot is shown in Figure 12 for MTB-DPP. The phenyl rings are twisted asymmetrically by about 12.2° and 11.1° in opposite directions with respect to the heterocyclic ring system. The heterocyclic ring system is not entirely planar but is folded in the middle with a dihedral angle of about 177.7°. Figure 13a shows the projection onto the (*a*,*b*) plane. The molecules are stacked in a fashion bricks in a brick wall, exactly as in MX-DPP (Figure 11a). Along the *b*-axis, as shown in Figure 13b, there are chains of intermolecular hydrogen bonds between the NH group of one molecule and the O atom of the neighboring one as in MX-DPP.

Figure 14 a and b shows the molecular stack on the (*a*,*b*) plane for MX-DPP and MTB-DPP, respectively. In MX-DPP, the *tert*-butyl group of one BTB-DPP molecule faces the phenyl ring of the neighboring DPP molecule in the lattice plane. The molecular environment characterized by two pairs of "*tert*-butyl group and phenyl ring" (in other words, local similarity in Figure

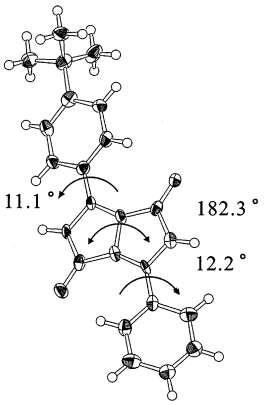

Figure 12. Molecular conformation of MTB-DPP.

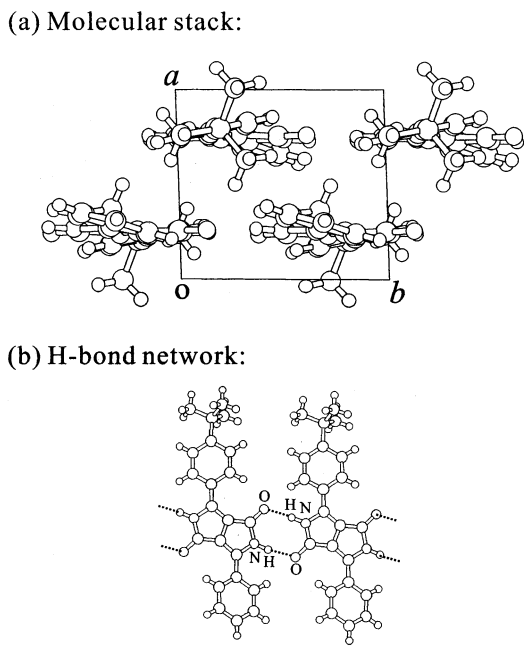

Figure 13. (a) Projection onto the (*a*,*b*) plane in MTB-DPP and (b) H-bond network of MTB-DPP on the molecular plane.

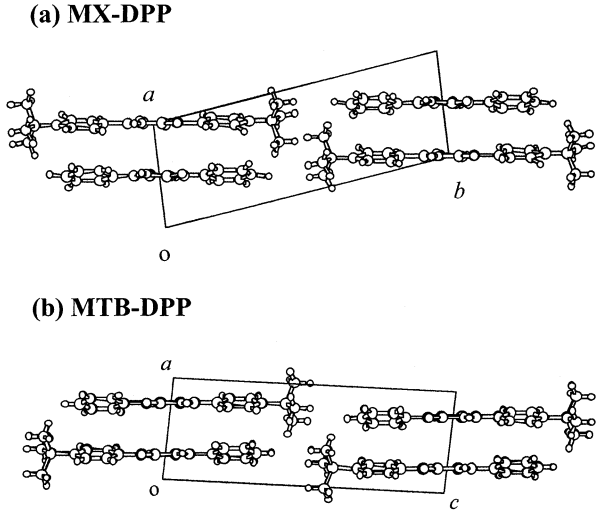

Figure 14. Molecular stack on the (*a*,*b*) plane: (a) MX-DPP and (b) MTB-DPP.

2a) is formed as suggested by Karfunkel and Mizuguchi et al.[8] Furthermore, the powder diffraction diagrams presented in ref 8 are in good agreement with the result of the present structure

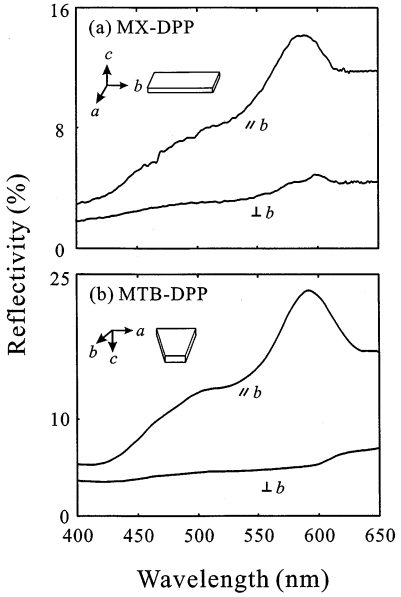

Figure 15. Polarized reflection spectra measured on single crystals: (a) MX-DPP and (b).

analysis. Similarly, in MTB-DPP, the *tert*-butyl group of one molecule faces the phenyl ring of the neighboring one as observed exactly in MX-DPP. The "local similarity" is clearly recognized as shown in Figure 2b. Here again, the powder diffraction diagrams of MX-DPP[8] are in good agreement with the result of the present structure analysis.

In summary, the present structure analyses of MX-DPP and MTB-DPP are basically in agreement with the result simulated by Karfunkel and Mizuguchi et al.,[8] although the *c* lattice of MX-DPP (18.36 Å) is nearly half of the simulated one (37.0 Å).

Polarized Reflection Spectra Measured on Single Crystals. Figure 15 a and b shows the polarized reflection spectra measured on single crystals of MX-DPP and MTB-DPP by means of a microscope spectrophotometer, respectively. In MX-DPP, reflection measurements were made on the (*a*,*b*) plane whose projection is shown in Figure 11. In MX-DPP, a prominent band appears around 585 nm for polarization parallel to the *b* axis. The present reflection spectrum is in good agreement with the absorption spectrum of evaporated MX-DPP after vapor treatment. On the other hand, the intense band is quenched for polarization perpendicular to the *b*-axis. The fact that the bands appear and disappear for different polarizations indicates that the transition dipole of MX-DPP points along the *b*-axis, that is, the direction of the intermolecular hydrogen bonds. This also agrees with the result of MO calculations.

In MTB-DPP, reflection measurements were made on the (*a*,*b*) plane whose projection is shown in Figure 13. The reflection spectra of MTB-DPP are similar to those of MX-DPP. A prominent reflection band appears around 600 nm together with a reflection shoulder around 480 nm for polarization parallel to the *b*-axis. The present reflection spectrum is in good agreement with the absorption spectrum of evaporated MTB-DPP after vapor treatment. On the other hand, the reflection bands are completely quenched for polarization perpendicular to the *b*-axis. This result evidently indicates that the transition dipole of MTB-DPP points along the *b*-axis, that is, the direction of the intermolecular hydrogen bonds. The present direction of the transition dipole is also borne out by MO calculations.

The above coincidence of both polarized reflection spectra of MX-DPP and MTB-DPP is obviously attributed to the same molecular environment (local similarity) in both crystals.

3.3. Excitonic Interactions on the Molecular Plane and along the Stacking Axis. We now discuss the electronic structure of the absorption spectra after vapor treatment composed of three absorption bands: 480, 540, and 580 nm (Figures 3 and 8).

As seen from the molecular arrangement shown in Figures 11 and 13, there are two kinds of intermolecular interactions in the crystal lattice: one is NH···O hydrogen bond interactions on the molecular plane and the other is $\pi-\pi$ interactions along the stacking axis. The major intermolecular interactions in pigments that determine the color in the solid state have been already clarified as arising from interactions between transition dipoles in pyrrolopyrroles,[2,13−15] phthanocyanines,[16,17] quinacridones,[18] and perylenes.[19,20] In particular, the J-aggregate-like structure in a fashion bricks in a brick wall[12] exhibits an extraordinary bathochromic shift in biphenyl DPP[13] and thionated DPP.[14,15] The mechanism of the large bathocrhomic shift due to the brick-wall structure can be summarized as follows.

When an excitation induces a transition dipole in the molecule, the excited state in crystals involves wave functions with significant probabilities on nearest neighbors. Therefore, the exciton coupling may well involve energy contributions from interactions with all of these nearest neighbor molecules acting in concert in the lattice. This may lead to a band splitting of the excited state or spectral displacement toward longer wavelengths or shorter wavelengths. The interaction energy ($\Delta E_{\text{exciton}}$) is given by the dipole−dipole equation:[21,22] $\Delta E_{\text{exciton}} = |\mu_T|^2(1 - 3\cos^2\theta)/r^3$, where the transition dipole is denoted by μ_T, the distance and angle between two transition dipoles by r and θ, respectively. As evident from the present equation, the overall spread or shift energy is determined by the strength of the interneighbor coupling ($|\mu_T|^2$) which directly depends on the absorption coefficient of the molecule as well as the mutual relative orientation of the transition dipoles in molecular assemblies. That is, the term ($1 - 3\cos^2\theta$) determines the geometrical relationship of transition dipoles correlated with the crystal structure. The bathochromic or hypsochromic shift depends on the critical angle of $\theta = 54.7°$, below which the former will result and above which the latter will be the case. The maximum bathochromic or hypsochromic shift is achieved by "head-to-tail" arrangement or "parallel" arrangement, respectively.

On the basis of the present exciton theory, we will consider the spectral shifts in MX-DPP and MTB-DPP with the direction of the transition dipole in mind, that is, the direction along the intermolecular hydrogen bond (Figures 11 and 13). It is then apparent that the intermolecular NH···O hydrogen bond serves to align the transition dipoles in a way "head-to-tail", leading to a large bathochromic shift of the absorption band. This corresponds to the spectral shift on going from solution to the solid state in evaporated films before vapor treatment (Figure 3).

As soon as the molecules are ordered, because of vapor treatment, along the stacking axis in a fashion bricks in a brick wall structure (Figures 11 and 13), an additional interaction arises from the diagonal molecule pairs along the stacking axis. The slip angle between the transition dipoles amounts to about $\theta = 43°$ which is below the critical angle of 54.7°. This causes an additional bathochromic band to appear around 580 nm. The final absorption band is therefore the superposition of three bands: 480, 540, and 580 nm. The spectral transition from two bands (480 and 540 nm) to three bands (480, 540, and 580 nm) is clearly shown in Figure 8. Since the bricks in a brick wall structure is specific of MX-DPP and MTB-DPP and is not found in ordinary DPP compounds,[2] the absorption spectra of ordinary DPPs are usually composed of only two absorption bands around 480 and 540 nm.[2]

As described above, the longest-wavelength bands in MX-DPP and MTB-DPP are correlated with molecular arrangement along the stacking axis. Since the intermolecular interactions are supposed to be enhanced because of lattice contraction at low temperatures, the temperature dependence of absorption spectra is a good measure for the characterization of the electronic transition that is associated with molecular arrangement. In DPP compounds with the bricks in a brick wall,[14] the lattice contraction predominantly occurs along the stacking axis while the rigid H-bond network is quite insignificant for temperature variations. In fact, an appreciable temperature dependence is observed in both absorption spectra in MX-DPP and MTB-DPP as shown in Figure 6. The present temperature dependence is quite similar to that of thionated DPP which crystallizes with the brick-wall structure.[14]

3.4. Driving Force for the Formation of the 1:1 Mixed Crystal. Since the MTB-molecule is an asymmetric molecule characterized by a small dipole moment of 0.16 D,[5] the molecules are considered to be arranged pairwise so as to reduce the electrostatic energy to form the molecular environment of *tert*-butyl group and phenyl ring. It is also expected that the present arrangement is sterically convenient for a high-density packing which also results in a high lattice energy. On the other hand, DPP and BTB-DPP are symmetrical molecules which have no dipole moment. Nevertheless, the molecules form the 1:1 mixed crystal with a similar molecular arrangement of MTB-DPP. Although details on the driving force for the 1:1 molecular arrangement are not yet fully understood, it is assumed that the steric effect is the major factor which governs the molecular arrangement and that the dipole moment as found in MTB-DPP plays no noticeable role in the molecular packing of MX-DPP.

3.5. Similar Mixed Crystals in Pyrrolopyrroles and Quinacridones. The spectroscopic and crystallographic similarities between MX-DPP and MTB-DPP presented here is one of the examples found in pyrrolopyrrole and quinacridone compounds. Apart from the present case, DPP and *p*-Cl DPP (chlorination at the para-site of the phenyl ring), for example, form a 1:1 mixed crystal whose electronic spectra and X-ray diffraction diagrams are quite similar to those of their hybrid compound. Details of the examples are given in refs 6 and 7.

4. Conclusions

The electronic structure of MX-DPP and MTB-DPP in evaporated films as well as in single crystals has been investigated from the standpoint of the crystal structure and intermolecular interactions. The conclusions of the present investigation can be summarized as follows.

1. MX-DPP and MTB-DPP exhibit surprisingly similar spectroscopic and crystallographic characteristics in evaporated films as well as in single crystals.

2. The absorption spectra of evaporated MX-DPP and MTB-DPP before vapor treatment are typical of ordinary DPP derivatives peaking around 540 nm. This is due to the two-dimensional H-bond network which aligns the transition dipoles in a way "head-to-tail", leading to a bathochromic shift upon crystallization. An additional spectral displacement is brought about by vapor treatment in MX-DPP and MTB-DPP which

forms the brick wall structure along the stacking axis. Because of this, the longest-wavelength band in MX-DPP and MTB-DPP is positioned at a longer wavelength as compared with that of ordinary DPP pigments which have no brick-wall structure.

3. In single crystals of MX-DPP and MTB-DPP, the crystal system and the space group are the same (monoclinic and $P\bar{1}$) and the lattice parameters are also quite similar. In both MX-DPP and MTB-DPP, the molecules are stacked in a fashion bricks in a brick wall. The local similarity as characterized by two pairs of *tert*-butyl group and phenyl ring prevails throughout the crystal in both compounds. The local similarity is concluded to be the key factor for the coincidence of the optical and structural properties between MX-DPP and MTB-DPP.

References and Notes

(1) Iqbal, A.; Cassar, L.; Rochat, A. C.; Pfenninger, J.; Wallquist, O. *J. Coat. Tech*. **1988**, *60*, 37.
(2) Mizuguchi, J. *J. Phys. Chem. A* **2000**, *104*, 1817.
(3) Mizuguchi, J.; Grubenmann, A.; Rihs, G. *Acta Crystallogr*. **1993**, *B49*, 1057.
(4) Mizuguchi, J. *Acta Crystallogr*. **1998**, *C54*, 1482.
(5) Mizuguchi, J.; Shikamori, H. *Z. Kristallogr. NCS* **2002**, *217*, 515.
(6) Mizuguchi, J.; Hao, Z. U.S. Patent 5,693,824, 1997.
(7) Hao, Z.; Iqbal, A. U.S. Patent 5,708,188, 1998.
(8) Karfunkel, H.; Wilts, H.; Hao, Z.; Iqbal, A.; Mizuguchi, J.; Wu, Z. *Acta Crystallogr*. **1999**, *B55*, 1075.
(9) Mizuguchi, J. *Krist. Tech*. **1981**, *16*, 695.
(10) Zerner, M. C. *ZINDO: A General Semiempirical Program Package*; Department of Chemistry, University of Florida: Gainesville, FL.
(11) Mizuguchi, J.; Shikamori, H. *Z. Kristallogr. NCS* **2003**, *218*, 127.
(12) Kobayashi, T. *J-Aggregates*; World Scientific Publishing Co. Pte. Ltd., 1996.
(13) Mizuguchi, J. *J. Imag. Sci. Technol.* **2002**, *46*, 257.
(14) Mizuguchi, J.; Rochat, A. C.; Rihs, G. *Ber. Bunsen-Ges. Phys. Chem.* **1992**, *96*, 607.
(15) Mizuguchi, J. *Electrophotography* (Denshi Shashin) **1998**, *37*, 58.
(16) Mizuguchi, J.; Matsumoto, S. *J. Phys. Chem. A* **1999**, *103*, 614.
(17) Endo, A.; Matsumoto, S.; Mizuguchi, J. *J. Phys. Chem. A* **1999**, *103*, 8193.
(18) Mizuguchi, J.; Endo, A.; Matsumoto, S. *J. Imag. Soc. Jpn.* **2000**, *39*, 94.
(19) Mizuguchi, J. *J. Appl. Phys.* **1998**, *84*, 4479.
(20) Mizuguchi, J.; Tojo, K. *J. Phys. Chem. B* **2002**, *106*, 767.
(21) Kasha, M. *Spectroscopy of the Excited State*; Plenum Press, 1976; p 337.
(22) Craig, D. P.; Walmsley, S. H. *Excitons in Molecular Crystals*; W. A. Benjamin, Inc., 1968.